Progress In Electromagnetics Research, PIER 41, 307–335, 2003

THREE DIMENSIONAL PHOTONIC CRYSTALS IN THE VISIBLE REGIME

T. Maka, D. N. Chigrin, S. G. Romanov and C. M. Sotomayor Torres

Institute of Materials Science
and Department of Electrical and Information
University of Wuppertal
Gaußstr. 20, 42097 Wuppertal, Germany

Abstract—3-dimensional photonic bandgap structures working in the visible have been given increasing attention in recent years encouraged by the possibility to control, modify or confine electromagnetic waves in all three dimensions, since this could have considerable impact on novel passive and active optical devices and systems.

Although substantial progress has been made in the fabrication of 3D Photonic crystals by means of nano-lithography and nanotechnology, it still remains a challenge to fabricate these crystals with feature sizes of the half of the wavelength in the visible. Self-assembling of colloidal particles is an alternative method to prepare 3-dimensional photonic crystals. The aim of this article is to show how to use colloidal crystals as templates for photonic crystals and how to monitor the changes of their optical properties due course of the modification.

1. INTRODUCTION

Since the first proposal in 1972 by V. P. Bykov [1] and in the late 80s by E. Yablonovich and S. John [2] photonic crystals have been gaining much interest both for fundamental and applied research. Photonic crystals (PhCs) or photonic bandgap (PBG) materials are periodic dielectric structures that are designed to form the energy band structure for photons, which either allows or forbids the propagation of electromagnetic (EM) waves of certain frequency ranges in the same manner as the periodic potential does for electrons in atomic crystals. The energy bandstructure for photons give rise to distinct optical phenomena such as the localisation of photons, the inhibition of the spontaneous emission, the ultra-refraction, etc. Indeed, the most interesting applications of photonic crystals for optoelectronics are expected in the near-IR and the visible parts of the spectrum. Naturally, to exploit the photonic crystal in its full capacity, it should be able to cope with EM waves of arbitrarily mode structure what, certainly, calls for 3-dimensional PBG structures.

Complete PBGs, meaning an omnidirectional gap and vanishing density of photonic states (DOSP) inside the photonic crystal, cannot be expected for any finite size systems. Nevertheless, a suppression by several order of magnitudes can be expected from defect free crystals and is sufficient for practical applications.

To obtain a 3-dimensional PBG in the visible, periodic ensembles of scatterers, whose lattice parameters are comparable to the half of the wavelength, have to be realised. Although considerable progress has been made in recent years to microfabricate structures in the sub-μm regime, this constraint still possesses a hard challenge to artificially made photonic crystals. Efforts in fabrication of 3D periodic structures are divided between sequential and parallel processing. The first approach is represented by nanolithographic patterning and subsequent layer-by-layer assembling of 2-dimensional structures,

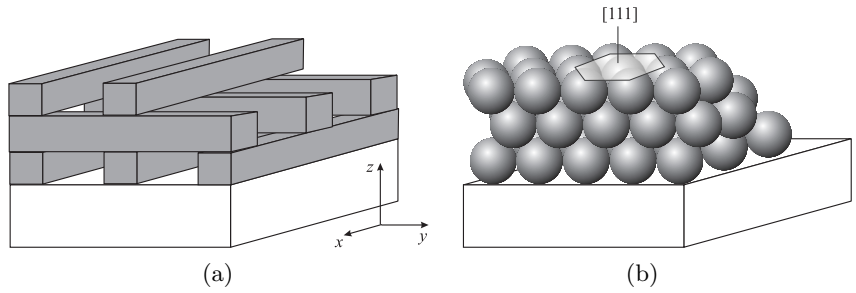

Figure 1. Schematic illustrations of the woodpile structure (a) and the self-assembled closed-packed cubic fcc structure of opaline photonic crystals (b). The woodpile structure is a popular candidate for layer-by-layer micro-fabrication processes.

e.g., by wafer fusion technique (Fig. 1(a)). Other approaches use x-ray lithography, focused ion beam etching in macroporous silicon, electrochemical etching, autocloning, 4 beam mixing using photopolymers, etc. to introduce the nanoscale 3-dimensional pattern in the bulk material [3–8]. Alternative processing relays on the self-organisation of individual nanoscale scatterers in large ordered ensembles (Fig. 1(b)). One prominent example of a self-assembled photonic crystal is artificial opal. In what follows we will discuss some problems related to the development of opal-based photonic crystals and to the optical studies of these structures.

2. OPAL STRUCTURE

Opals are naturally occurring 3-dimensional periodical packages of monodisperse a-silica spheres arranged in a face centred cubic (fcc) lattice. Their structure was first mimicked artificially in the 70s (Fig. 1(b)). The diameters of the spheres in opal can be varied from 150 nm to 1 μm, thus the Bragg resonance can cover the range of optical frequencies from near infrared (NIR) to the ultraviolet (UV). Opals with periods of 200–350 nm show photonic band gaps in the visible region of the spectrum, 1.9–2.6 eV.

The synthesis of monodisperse silica spheres is mostly based on the Stöber process [9]. To fabricate opals, these spheres are sedimented subsequently to form ordered packages which are sintered afterwards [10]. Sedimentation under gravitational force works well for a limited range of sphere diameters from ca. 200 to 550 nm. Sedimentation of small spheres on the one hand (diameter $<$ 200 nm) can lead to very long settling times of several month, or, on the other hand,

sedimentation of big spheres (diameter $>$ 550 nm) leads to high sedimentation velocities which prevent a good long range fcc ordering.

To produce high-quality crystals, the sedimentation velocity has to be controlled. To achieve this, for example an electrophoretic approach has been introduced as a means to improve the monocrystallinity of opals [11]. By applying an electric field the sedimentation velocities of silica spheres can be changed by will, allowing the synthesis of photonic crystals with a wider range of sphere diameters. With this method it is possible to synthesise high-quality opaline crystals with diameters up to 1000 nm, consequently realising photonic structures beyond the visible and NIR range.

The crystallinity of bulk opals is intrinsically limited by the self-organising nature of the sedimentation process. Usually there is about 1 defect per 100 unit cells. Moreover, stacking faults disturb the ABCABC... sequence and give rise to distorted PBG properties [12]. Thus, disorder remains one of the key problems in self-assembled systems.

Latex beads, e.g., PMMA or polystyrene, are an alternative to silica spheres and allow the extension to a variety of structures [13]. Polymers can be easily doped with light emitting species prior to the sedimentation, modified by deposition of functional groups or made into nanostructured media themselves by deposition of inorganic shells [14]. Photonic crystals can be fabricated from these polymeric beads similar to silica-based opals.

3. OPTICAL DIFFRACTION IN OPALS

Optical studies of opals as photonic crystals were launched in 1995 [15–16]. Reflection and transmission measurements are commonly used to probe the crystalline structure of photonic crystals. They are performed by illuminating a specific area of the surface ($\sim$ mm^2) of the specimen with white light and collect the reflected light within a small ($\sim$ 1°–5°) solid angle. As shown in Fig. 2, the optical transmission and reflectance spectra of opal contain diffraction resonances, which appear at one and the same frequency either as dip or maximum (Fig. 2(a)). The following parameters of this diffraction resonance can be defined: the resonance frequency ($E_B = \hbar\omega_B$), the full width at the half-maximum (FWHM), the depth of the transmission minimum and the resolution of the reflectance maximum. Another important parameter is the overlap of these diffraction resonances recorded at different angles of observation (Fig. 2(b)), which feature can be used to characterise the completeness of the PBG structure. The spectral position of the resonance is trivially defined by the Bragg condition

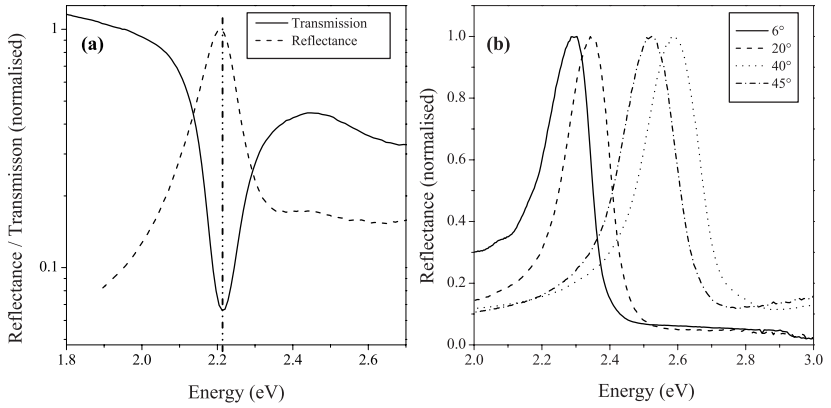

Figure 2. Typical Reflectance and Transmission spectra of opal-based photonic crystals: Transmission and Reflectance spectra at normal incidence. The Bragg resonance appears as a dip in the transmission at the same energy as the Peak in the reflectance spectrum (a). Angular resolved Reflectance measurements: The shift of the Resonance follows the Bragg law. The overlap of two spectra recorded at different angles and the FWHM of the peaks are important characteristics (b).

$\lambda_B = 2d\sqrt{n_{\text{eff}}^2 - \sin^2\theta}$. Its position can be varied by changing the lattice parameter d, the angle of incidence θ and the effective index of the refraction n_{eff}. This value is determined by an effective medium approach $n_{\text{eff}}^2 = f_1 n_1^2 + f_2 n_2^2 + \cdots + f_n n_n^2$, with f_i and n_i representing the filling fractions of the different constituents and their refractive indices, respectively. In contrast to the spectral position of the Bragg peak, the width of the resonance, which relates to the dielectric contrast, and its resolution, which is connected to the crystallinity of the opal, are subjects of thorough investigations and clever material design. This is because, firstly, the self-organisation produces ensembles of scatterers, which are ordered statistically but not explicitly, and, secondly, the colloidal crystallisation is known for particles made from a limited number of materials.

To improve the optical data, single domain spectroscopy of a polycrystalline opal was suggested. In particular, micro-reflectance spectroscopy — projecting the microscope image of the sample into a spectrometer — has been employed by Vlasov et al. [17]. Obviously, the drawback of microdiffraction measurements is the dependence of the results upon the choice of a particular domain. In following sections we will show how to tackle with ordering of opals and how to deal with the issue of the refractive index contrast.

4. SYNTHESIS OF OPALINE FILMS

The depth of the transmission minimum produced by one monolayer of packed spheres is limited by their scattering strength, which in turn is a function of the dielectric contrast. Numerical modelling shows that not more than 5 successive layers of Si-made scatterers are necessary to complete the formation of the optical stop-band resembling that of an infinite photonic crystal. Correspondingly, where photonic crystals of full PBG are concerned, there is no reason to construct thick packages of scatterers.

From the other hand, after first attempts to mimic the naturally occurring bulky opals, the growth of opals as thin coatings has been suggested as the means to improve the crystallinity of the sphere package. One advantage of a thin film opal over its bulky counterpart is the orientation of the crystallites in the film with the [111] axis normal to the surface. Besides, the improved area to volume ratio in the films leads to fewer defects. Moreover, pre-patterned substrates can be used to control the symmetry of these thin-film opals [18].

The straightforward formation of polymer opaline films has been made by casting a suspension of PMMA beads, prepared by a modified emulsion polymerisation [19], on hydrophilic substrates. By drying the suspension in an atmosphere of controlled humidity (98%), opaline films covering areas of several cm^2 can be prepared. The beads are organised in an fcc package with the [111] direction normal to the substrate. These thin-film photonic crystals consist of about 20–50 monolayers of beads, and possess domains of 10 μm to 500 μm (Fig. 3). SEM inspection shows that the long-range order of the crystallites is preserved over the cracks in the area of up to several cm^2, thus leading to the assumption that cracks are formed during the drying process of the crystal. In general, thin film PMMA-based opals combine the advantage of a cheap and quick synthesis with easy machinability and good mechanical stability.

Opaline films should be made ideally with a controllable number of layers. Thin film photonic crystals, the thickness of which is controlled by growing them in physically confined cells under sonic agitation, were prepared successfully by Gates, Xia et al. [20]. A different method was suggested by Kralchevsky et al. [21], who used capillary forces to construct opaline films from colloidal suspensions on vertical substrates. Apart from better crystallinity, this method allows to change the number of monolayers simply by changing the bead concentration in the suspension.

Application of alternate external force during the crystallisation of the colloid, particularly, shear alignment, has been suggested to

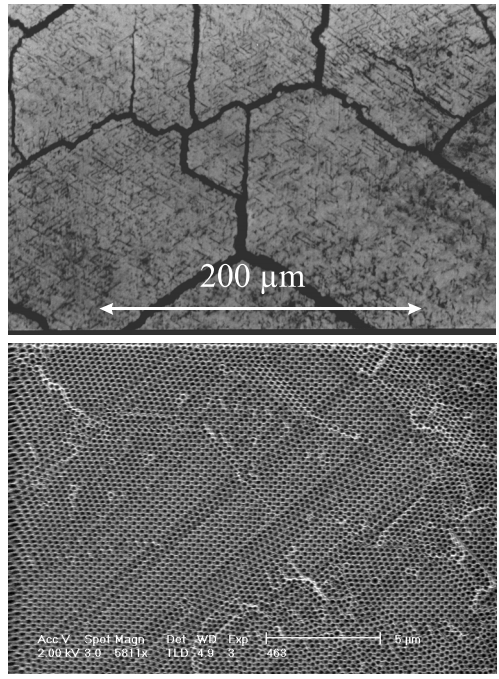

Figure 3. Microscopic image of a PMMA based photonic crystal (Top) and SEM micrograph (bottom). Note the large domain size and well established long range ordering.

enhance the crystallinity of opals and to produce large-area ($\sim$cm^2) defect-free opaline crystals [22]. Illuminated with monochromatic light, these crystals show the prominent, Laue-like, pattern in transmission. The long-range order in the form of predominantly twinned fcc lattice was confirmed by observation of the Laue diffraction from the whole area of the crystal. However, since PMMA beads are subject to shrinking during the evaporation of the solvent, these films break up into smaller domains of $\sim$ 100 μm during the drying process. This makes their handling and post-processing cumbersome and limits the possible application.

It is widely acknowledged that the homogeneity of opals is critical to obtain distinct photonic bandgaps. Crystallite sizes up to 0.5 mm in bulk opals [23] and several square millimetres in films [24] are reportedly the best results so far.

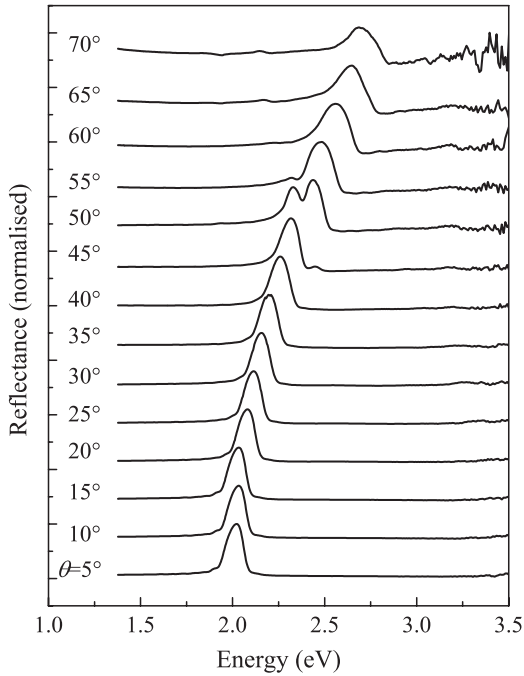

Figure 4. Bragg reflectance peaks from a PMMA thin film photonic crystals. For angles between 45° and 55° a splitting of the reflectance peak into 2 branches is observed. The curves are normalised and shifted vertically for clarity [28].

5. CONSEQUENCES OF IMPROVED QUALITY

Reflectance spectra of a representative PMMA opaline film collected at different angles θ are shown in Fig. 4. They were performed for an angular range from $\theta = 5°$ to 70° in the Bragg configuration, where the angle of incidence is equal to the angle of collection of the reflected light. The relative stop-bandwidth of $\Delta E/E_0 \approx 5\%$ can be determined as the FWHM from the Bragg resonance at near normal incidence ($\theta \approx 5°$). This value matches well with the 6.3% FWHM of the [111] relative gap width calculated by the plane wave method [25]. This agreement is, probably, due to the relatively low contribution from defects of the photonic crystal films.

The indicator for the quality of thin film photonic crystals is the occurrence of interference fringes in the reflectance spectrum (Fig. 5). These oscillations can be understood as Fabry-Pérot oscillations occurring due to the interference of the light reflected by opposite

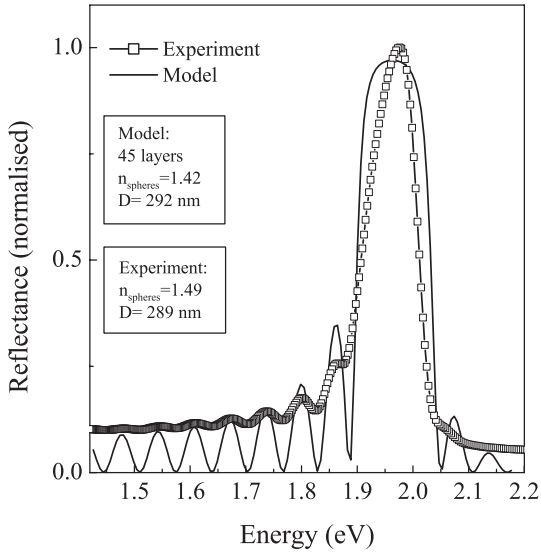

Figure 5. Bragg resonance of a PMMA thin film PhC. The reflectance measurements show Fabry-Pérot oscillations. We consider beads with a diameter of 292 nm in good agreement with SEM images. Measurements (squares) and simulation (line) show excellent agreement [28].

surfaces of the opal domains. Fabry-Pérot oscillations are a good indicator of the homogeneity of thickness and average RI of photonic crystals since otherwise they will vanish rapidly. In the case of thin opaline films Fabry-Pérot oscillations have been routinely observed from a spot up to 1 cm^2, indicating the high crystallinity of these films compared to bulk opals [28], where the single domain spectroscopy is necessary. Quantitatively, with increasing the spot area from 1 mm^2 to 1 cm^2, the magnitude of Fabry-Pérot oscillations reduces approximately by factor of three.

Remarkably, the Fabry-Pérot oscillations appear different from both sides of the Bragg resonance showing a rapid decrease of the oscillation magnitude on the high-energy side. The evolution of the amplitude of Fabry-Pérot oscillations can be explained by a rapid variation of the dielectric properties of the material in the vicinity of the photonic band gap.

The reflectance spectra of films with different number of layers were calculated by using a 3-dimensional transfer matrix method [26]. The calculated period of the Fabry-Pérot oscillations was found to

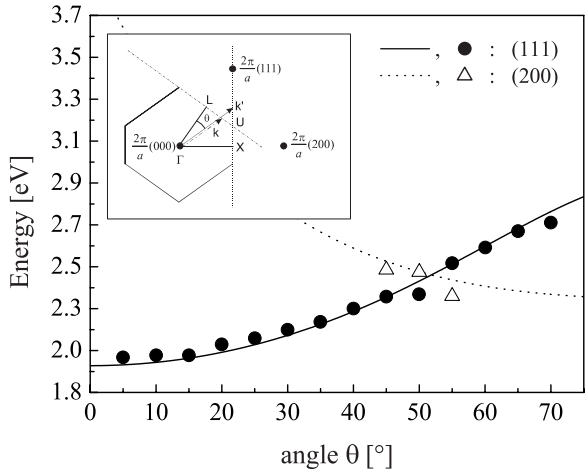

Figure 6. Comparison of the angular dependence of (111) and (200) Bragg Peaks. Experimental data (• for (111) and △ for (200)) and theoretical calculations (solid and dashed lines). The inset shows the (ΓXL) plane of the fcc Brillouin zone in reciprocal space. The dotted and dash-dotted lines indicate positions for the wave vectors k and k', where the condition for refraction at (111) and (200) planes is satisfied. For the given incident angle θ this is the case for both vectors k and k', thus a two reflection peaks can be found near the U-Point [28].

coincide with experimental values for a film thickness of 45 bead layers as depicted in Fig. 5, which compares the experimental and theoretical reflectance curves. The diameter of the spheres as determined by SEM inspection to be $D = 289$ nm also compares well to the modelled value of $D = 292$ nm. For energies below the gap, the amplitude of the calculated oscillations increases towards the Bragg resonance and rapidly decreases above it, which is in a good qualitative agreement for the observed evolution. It is worth mentioning that a one-dimensional model of the reflection properties does not reproduce the variation of the Fabry-Pérot oscillation amplitude correctly. The good agreement with theory, which assumes perfect arrangement of spheres, underlines the high order quality of the thin film sample [28].

A split in the Bragg resonance was observed for external angles between $\theta \approx 45°$ and 55° (Fig. 4) in reflectance measurements similarly to that reported from high quality TiO_2 replicas by van Driel and Vos [27]. The measurements were performed using unpolarised light. Fig. 6 shows the angular dependence of the Bragg resonances from (111) and (200) planes for a PMMA opal film together with the theoretical

evolution of the corresponding Bragg resonances for different angles. The dots represent data that can be linked with reflections from (111) planes, whereas triangles can be associated with reflections from (200). For incident angles θ between 45° and 55° the Bragg condition is nearly satisfied for both, plane sets. The inset of Fig. 6 shows this situation in the reciprocal space. For all k-vectors ending on the dotted or dash-dotted lines the diffraction condition for (111) or (200) planes is fulfilled, consequently both reflections can be observed.

It is evident, that peaks associated to the (111) diffraction can be observed in a big angular range, whereas peaks associated to the (200) diffraction can only be observed in a small angular interval. More detailed calculations show that the gap for (111) diffraction is open for a large range of k-vectors along the LU-line, whereas the gap for (200) reflection exists only in the vicinity of the U-point. This gives a clear explanation for the existence of double peaks only for angles near $\theta = 51.84°$, which corresponds to the U-direction. A more detailed description can be found in [28].

The experimentally observed positions of the are in agreement with the theoretical predictions but the deviation from the theoretical curves near the crossing point cannot be explained based on the simple Bragg law. Presumably, multiple band branching that occurs at the U-point decreased the frequency of the bands. This phenomenon is well known from solid state physics and explains the deformation of the bands and thus the deviation from the Bragg law.

No doubling was found for p-polarised waves, in contrast to s-polarised waves, where a pronounced splitting is observed. This seems to reflect the neighbourhood of the scattering centres and was confirmed by TMM modelling.

6. SYNTHESIS OF INVERTED OPALS

Achieving a high refractive index contrast (RIC) in photonic crystals is a crucial problem for the development of a complete PBG structure. The increase of the RIC leads to broadening of all stop-bands and to the development of a complete omnidirectional bandgap between the 8^{th} and 9^{th} bands in the fcc lattice of dielectric scatterers occupying about 30% of the photonic crystal volume [29] (Fig. 7). To enhance the RIC of opaline photonic crystals the filling of the matrix with semiconductors has been suggested. The subsequent removal of the matrix produces a so-called inverted opal structure ("opal replicas"). In accord with theoretical calculations to achieve a complete PBG the inverted opals made from materials of RI $\geq$ 3 have to be employed for defect-free crystals (Fig. 7(b)). Theoretical calculations show to

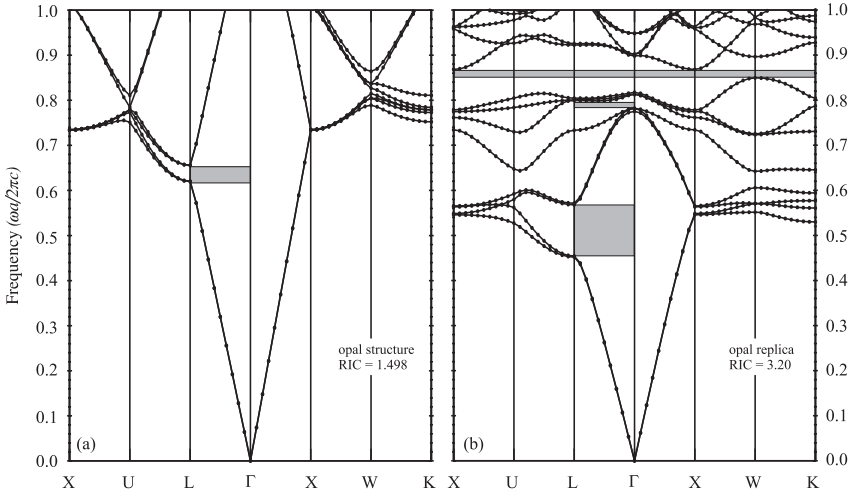

Figure 7. Photonic band structures of closed-packed fcc lattices of PMMA, $n = 1.498$. Balls in air (a) and air balls in a SnS_2-matrix, $n = 3.2$ (bulk value), (b). Partial bandgaps in [111] direction are marked in grey. For the SnS_2 replica (b) a full bandgap is present between the 8^{th} and 9^{th} bands (grey area). Band structures have been calculated by a modification of the planewave expansion method using a freely-available software package [48].

achieve an omnidirectional PBG, a RIC > 2.8 is necessary [30]. The complete gap is believed to be very susceptible to disorder, therefore a good margin by RIC contrast has to be kept.

Experiments to study replicas that approach the high RIC were done by several groups. First example of inverted opaline structure was presented by Wijnhoven et al. in inverted TiO_2 opal [31], whereas the first evidence of a full PBG in the IR has been reported in inverted Si-opal for the 1.5μm wavelength range [32]. To reach the visible part of the spectrum, the key problem is the limited choice of semiconductors, whose RI exceeds 2.8 and whose electronic bandgap is above ~ 2 eV. So far TiO_2 inverted opals were prepared mostly in the anatase form of 2.5 index of refraction instead of 2.8, characteristic for the rutile form. Besides, they suffer a low volume fraction of TiO_2, which value of about 10% is far below the 30% necessary for maximising the gap width [33]. Attempts to fill opals with GaP also have not yet led to sufficiently high filling factors to produce inverted structures [34]. SnS_2 inverted thin film opals are potentially promising photonic crystals operating in the visible. This semiconductor combines a 2.4

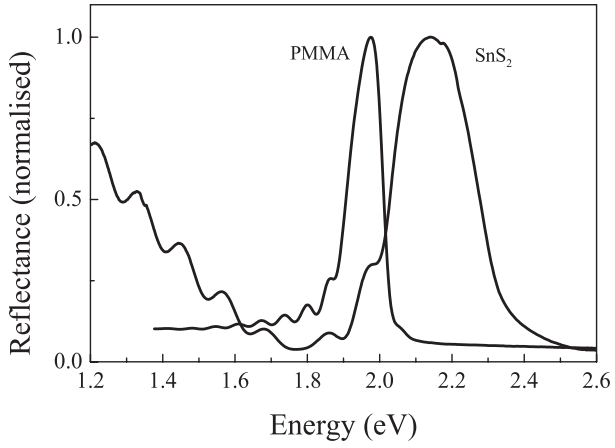

Figure 8. Reflectance spectra of PMMA opaline film from spheres with diameter $D = 289$ nm, $n = 1.49$ and its SnS_2 replica $n = 1.91$. The SnS_2 spectrum is shifted to the blue and broadened due to the increased effective RI and more optimal filling factor. Note the Fabry-Pérot oscillations on the low-energy side of the spectra indicating the good crystalline quality of both films.

eV-wide direct electronic gap (indirect electronic transition 2.1 eV) and is therefore interesting for the red part of the visible spectrum. It shows a bulk index of refraction of 3.2 at an energy of 1.8 eV. SnS_2 replicas are produced by chemical vapour deposition of SnS_2 into polymeric thin film opals. The synthesis is performed from $SnCl_4$ vapour and H_2S gas at room temperature and ambient pressure. By this method it is possible to infill the voids of the photonic structure in about 24 h. A slow reaction inside of the template is crucial to avoid a blocking of the voids in the peripheral regions of the template, which would result in a gradually diminishing filling factor towards the centre of the sample. The PMMA beads are dissolved subsequently using an organic solvent (THF), leaving behind the semiconductor replica on the glass substrate [35]. The absence of solid precursors and the moderate temperatures and pressures used by this method allow a sparing infill into a variety of different polymer templates without reducing the degree of order in the resulting replica too much. The replica is, as the template, uniform over an area of cm^2. A crucial point in the evaluation of inverted semiconductor opals is determination of the porosity of the infilled material to calculate the "real" filling factor, which limits the effective RIC. So far effective RIs between 1.9 and 2.7 have been realised experimentally.

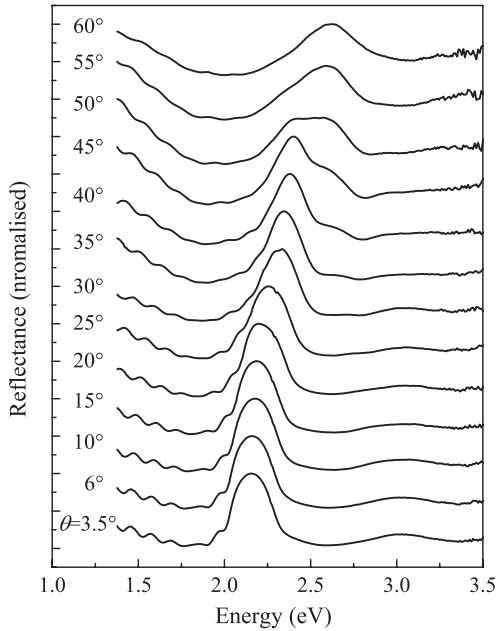

Figure 9. Reflectance spectra for a SnS_2 replica. Band branching can be observed for external angels θ between ca. 35° and 55° similar to PMMA templates (Fig. 4).

7. OPTICAL DIFFRACTION IN INVERTED OPALS

In comparison with the PMMA templates, in the SnS_2 films the Bragg resonance shifts to the blue with the change of the effective RI of the structure as a whole.

An obvious increase of the FWHM is achieved with the inversion of the PMMA opal as shown in Fig. 8, where the Bragg resonances from a PMMA template and its SnS_2 replica are compared. The FWHM of the Bragg Peak increases from 5 to 15% in the template, mainly due to the enhanced RIC.

SnS_2 replicas demonstrate an optical behaviour similar to their PMMA templates, namely Fabry-Pérot oscillations (Fig. 8) and band branching (Fig. 9). In particular, this indicates preserving a high level of ordering, characteristic for a template, during the inversion process.

The branching spans a larger range of angles in the case of SnS_2 replicas compared to PMMA templates. Additionally, a comparison of branching in PMMA and SnS_2 opaline films reveals much stronger band repulsion, moreover, the dispersion after the branching point loses

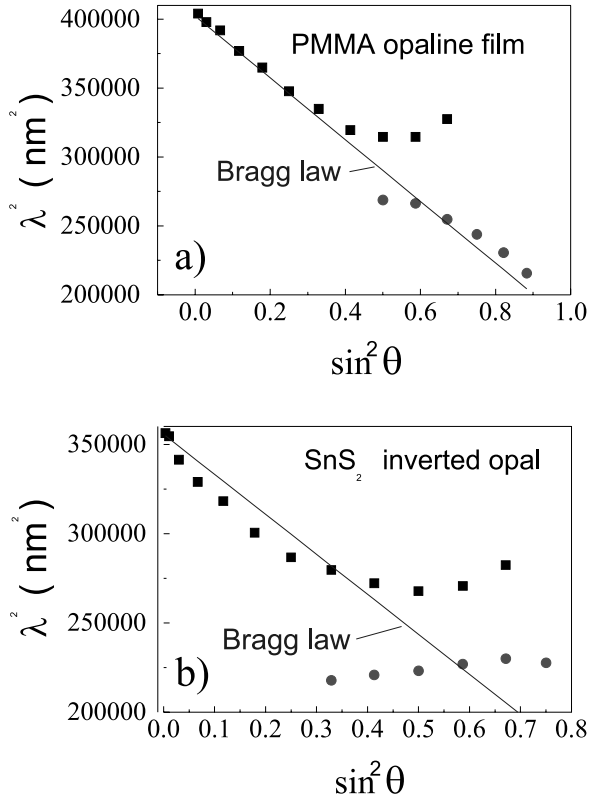

Figure 10. Band Branching in PMMA and SnS_2 opals. The SnS_2 samples exhibit a much stronger band repulsion and the dispersion looses the relation the Bragg law after the branching point.

its relation to the Bragg law (Fig. 10). Obviously, this is because of the higher RIC in the opaline replica.

8. LIGHT SOURCES

Emission studies from light sources embedded into photonic crystals have been undertaken for several years. To achieve significant advances of PBG light sources certain conditions are necessary:

- The RIC has to be high enough to ensure the efficient interaction between the light source and the structure
- The presence of a light source should not compromise the RI contrast. It should be incorporated either in the body of the

PhC or occupy only a small fraction of the internal volume (e.g., coatings spread over the internal surface of the crystal). Examples are:

a) The body of a PhC made out of bright emitting CdS nanoparticles [36]. This approach lacks tunability and sufficient RI contrast due to the low density of CdS.
b) Opals loaded with dye molecules [37] or rare earth ions [38] in the spheres or their replicas. They allow independent tuning of the PBG and the emission band, but are limited by the chemical compatibility of materials.
c) Opal and its replica with dye molecules attached to the inner surface of voids [39]. These approach offers good tunability but the emission efficiency is low and the lifetime of the dye molecule is compromised.

- The emitting component must have a long lifetime under strong laser pumping or electrical excitation.

The driving force of emission studies in photonic crystals is the possibility of enhancement or suppression of the spontaneous emission (SE). The physical reason for the difference in the spontaneous emission rate is the engineered profile of the density of photon states and the localisation of states in the vicinity of a PBG. The emission intensity is proportional to the DOSP multiplied by the emission rate. The latter is itself a function of the DOSP and the localisation of the optical mode. Correspondingly, there is no emission coupled to eigenmodes of PhCs in the PBG energy range. If there is a defect in a otherwise perfect photonic crystal lattice, its optical mode may fall within the PBG. In this case emission can be coupled with this defect mode but its intensity will decay exponentially away from the defect, since the mode is localised. The decay rate is actually the quality factor of the localised mode. The emission rate into the defect mode is enhanced in proportion to Q in accordance with the Purcell effect [40]. Nevertheless, the intentional formation of defects in opaline PhCs for the visible has not been reported, yet.

9. EMISSION FROM OPALINE STRUCTURES — GAP IN THE EMISSION VS. GAP IN THE TRANSMISSION

To probe the changes of the emission properties of embedded light sources, photoluminescence (PL) spectra were excited by an Ar^+-ion laser operating in cw mode. The excitation power was kept low to avoid the degradation of the dye emission. Photoluminescence spectra

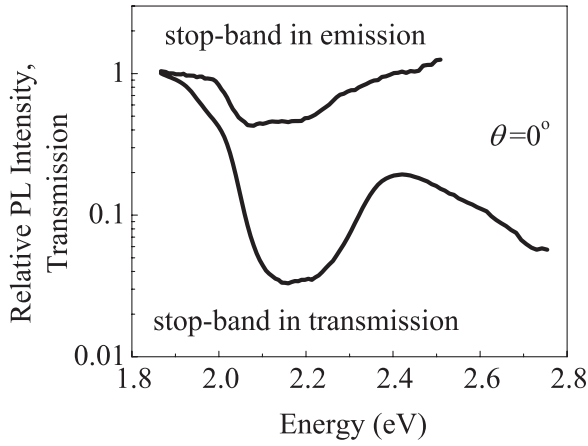

Figure 11. Relative PL and Transmission spectra from an inverted SnS2 thin film sample. The magnitude of the dip in transmission exceeds the dip in the PL spectrum by one order of magnitude.

were collected in transmission configuration from a small solid angle of $\sim 5°$ to exercise angular resolved measurements.

Two different samples were used, PMMA opal and SnS_2 inverted opal, to compare the PBG effect upon the emission.

PMMA based opaline films were doped with a Coumarin dye and SnS_2 inverted opaline films were loaded in a similar way with Perylene, by infilling of the dye solution into the voids. After evaporation of the solvent the dye remains attached to the inner surfaces of the voids. Laser dyes were chosen as emitting species because of their flexibility and uncritical handling. To match the emission spectrum of the embedded dye with the PBG, different dyes were chosen for PMMA opal and the SnS_2 replica, so a direct comparison can not be given. The Perylene dye was chosen for the SnS_2 replica because of its stability against degradation in the laser beam, but the spectrum appears more complicated for analysis.

PL spectra of dye-doped PMMA PhCs show clearly the partial suppression of the dye radiation intensity in these crystals for certain frequency ranges in the direction of observation [41–42]. The Bragg stop-band is in fact a partial PBG and therefore the emission is spatially redistributed, leading to an anisotropic emission pattern.

Remarkably, the depth of the stop-band in the PL is less than 50%, whereas the dip in the transmission spectrum of the same sample often exceeds two orders of magnitude (Fig. 11). The relative spectra shown in Fig. 11 were obtained collecting the transmission and PL spectra

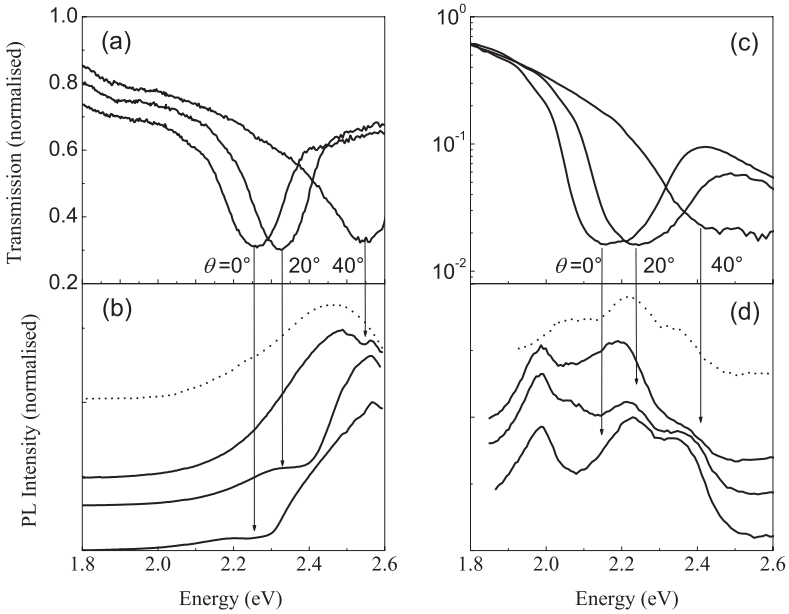

Figure 12. Photoluminescence of a PMMA photonic crystal (a), (b) and inverted SnS_2 film (c), (d) collected at angles 0°, 20° and 40° in comparison with transmission spectra at the same angles. The PL spectra of the reference samples are shown by dashed lines. Arrows show the central frequency of the stop-band at the angle of the emission collection indicated at each arrow. Curves in panels (b) and (d) are shifted vertically for clarity.

as well as reference spectra from unstructured samples of the same material and dividing the spectra by the reference to get the relative PL and transmission intensities, respectively. It appears that the emission from the near-surface region leaves the PBG structure unaffected and, additionally, that defects produce leakage modes within the PBG, thus allowing part of the emission to escape unaffected from the PhC.

Both, PMMA based opals and their SnS_2 replicas exhibit a similar spectral change of the suppression of the emission intensity with angular variation of the stop-band (Fig. 12).

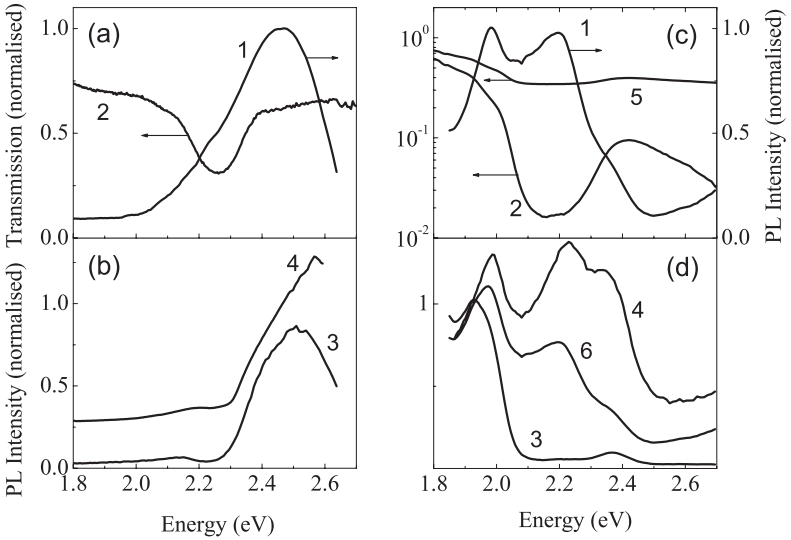

Figure 13. Reconstruction of PL spectra of PMMA and SnS_2 photonic crystals Panels (a), (c): PL spectrum of the reference sample (curve 1) and the corresponding transmission spectrum (curve 2) for these PhCs, respectively. Panels (b), (d) curves 3 — product of spectra 1 and 2. Curves 4 — experimental spectra. Closer fit to the experimental PL of perylene/SnS2 (curve 6) can be obtained with artificially reduced transmission spectrum (curve 5).

10. SPECTRAL REDISTRIBUTION OF THE EMISSION INTENSITY

Fig. 13(a) shows the transmission spectrum of a PMMA based thin film photonic crystal, which, practically, demonstrates the density of photonic states (DOSP) along the direction of emission collection, and the PL of a reference sample, which shows the spectrum of the light source in the free space. The product of these two spectra is supposed to simulate the effect of PBG on the spectrum of the light source. In fact, this simulation reproduces the experimentally observed PL spectrum very well (Fig. 13(b)). This suggests that changes in the spontaneous emission rate are too small to affect the appearance of the PL spectrum, so only a band-pass filtering occurs in accord with the transmission spectrum for these low RIC photonic crystals.

In contrast, a similar procedure applied to the SnS_2 sample leads to a different result (Fig. 13(c),(d)). If the transmission spectrum were applied in its full depth, the product of the reference emission and opal

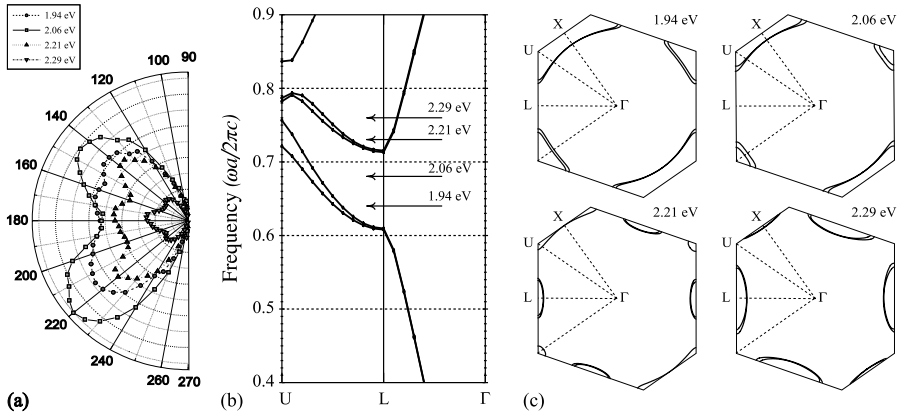

Figure 14. Angular PL diagram of SnS_2 inverted opal (a), the corresponding photonic band structure (b) and dispersion surfaces for different wavelength (c). The anisotropy of the emission corresponds to the anisotropy of the calculated dispersion surfaces.

transmission spectra would be entirely dominated by the minimum in the DOSP. However, with the transmission spectrum, which is artificially reduced by a factor of 10, it is possible to reproduce closer the experimentally observed PL spectrum. A remarkable feature is the 2.05 eV emission band. This band remains intact, when the stop band moves towards higher frequencies due course of changing the angle of the light collection. At higher angles 2.05 eV band cannot be simulated by this simple method, that is the manifestation of the enhancement of the emission rate at PBG edges. The obtained spectral redistribution is in agreement with theoretical calculations made for Bragg gap in high RI contrast PhC [43]. Thus, whereas a PMMA based opal seems to act mainly as a band pass filter, integrated with the light source, the emission of the SnS_2 sample acquires distinct features related both to the minimum in the DOSP and to the enhancement of the spontaneous emission rate.

11. DIRECTIONALITY OF EMISSION

Anisotropy is the most prominent feature of the emission from an incomplete PhC. The emission spectrum varies with changing the emission collection angle in agreement with the anisotropy of the stop-band (Fig. 14). In a periodic media the energy flow transported by EM wave is governed by the topology of the dispersion surfaces, the isofrequency surfaces in the k-space. In fact, the average Pointing

vector is parallel to the group velocity vector and so it is always perpendicular to dispersion surfaces [44]. For the energy range of Bragg stopband, the form of the dispersion surfaces is strongly different form the spherical mostly near the direction of the partial gaps. In the Fig. 13(c), dispersion surfaces for energies in the range of interest are presented. We have calculated the photonic band structure of the closed-packed fcc lattice of SnS_2 balls in air for all k-directions in the LUXΓ plane, using the method and software package of [48]. To obtain dispersion surfaces, we have computed the intersection of the 3D band structure with a plane corresponding to the wavelength of interest. In our calculations we assumed the effective RI of SnS_2 to be 2.1. This value was derived from measurements of the peak-shift in reflectance from the SnS_2 infilled structure compared to the polymer template [35]. The deviation from its bulk value is attributed to the porosity of the infilled semiconductor itself. The angular diagrams of emission intensity are in a good agreement with the topology of calculated dispersion surfaces, having pronounced dips in the directions of partial gaps and remaining close to the standard $\cos\theta$ like intensity distribution within the passbands.

12. CHANGES IN THE EMISSION RATE

The emission intensity depends on both the DOSP and the emission rate, moreover the latter is the function, partially, of the DOSP as well. Another variable, which determines the emission rate is the state of the localisation of the optical mode. In accord with the Purcell effect [45], the emission rate is directly proportional to the quality factor of localised states. In the case of low RI contrast opals, such localised modes relate to defects of the opal lattice, whose frequencies fall into the stop band. In this case the emission rate in defect modes can be either above or less as compared with the emission rate in propagating modes of PhC, which depends on the product of the quality factor and the mode density, whichever defect modes or eigenmodes are concerned. In order to obtain the spectrum of the emission rate, the DOSP was set constant by choosing a certain point in the sample and the angle of the light collection, and the power of excitation was made variable. Let us suppose that the emission rate is not the function of pumping. Then, after collecting PL spectrum at different excitation powers and dividing them by each other, we would find out that the ratio does not depend upon the frequency. However, experimentally found was the uneven spectrum, amplitude of whose features correlates with the position of the PBG. Supposing that the only parameter, which changes with the optical gain, is the spontaneous emission rate,

we can consider the ratio spectrum as the estimate of the emission rate spectrum. To avoid unnecessary complications the excitation power was chosen low, providing the absence of saturation effects. Intensity ratios of the PL spectra were calculated for excitation powers of 0.5, 1, 5 and 15 mW, giving power ratios of 30, 15 and 3 for the photonic crystal and 0.02, 0.2 and 2 mW for the unstructured SnS_2 reference film, as indicated in Fig. 15. The shaded region indicate the stop-band of the photonic crystal for different angles (0°, 30°, 60°). A ratio spectrum of the reference sample shows a similar ratio step at 2.4 eV which then gradually decays towards lower frequencies. This step, probably, indicates the onset of the radiative relaxation of the dye molecules, which appears due to an interplay between energy transitions in the excited dye molecule and in the SnS_2, because in the latter this energy is the electronic bandedge for direct transitions. In the PhC the ratio spectrum shows a dip at stop-band frequencies and a clearly visible band of enhanced spontaneous emission emerges at 2.4 eV. This band, which originates from the step in the reference sample, appears relatively stronger if it appears in the vicinity of the stop band edge. This observation is compatible to the theoretical forecast concerning the relative enhancement of the emission intensity being most pronounced at the high-energy edge of the photonic bandgap [43].

13. METALLODIELECTRIC OPALS

The gap-width-to-midgap-frequency ratio of the complete gap, which is a measure of the PBG width, is expected to be within 5% even in defect-free photonic crystals, which places a challenge to the fabrication of photonic crystals at optical wavelengths. Bearing this in mind, the use of dispersive materials has been suggested to build photonic crystals, in particular, metallodielectric (MD) nanocomposites. In contrast to the pure dielectric (DD) PhCs, MD structures are supposed to make the PBG a more robust effect. More important, MD PhCs have been predicted to tolerate a sufficient level of disorder and to lift off the refractive index contrast problem. The combination of both, dielectrics and metals in one MD PhC is anticipated to enhance the gapwidth-to-midgap frequency ratio dramatically to about 10% [46]. To date, no successful experiments have been reported with MD PhCs in the visible and the theoretical treatment suffers from some uncertainty.

Metals showing a Drude-like behaviour are typically lossy at optical frequencies except in a certain frequency window, where they behave as a conventional dielectric, although a highly dispersive one.

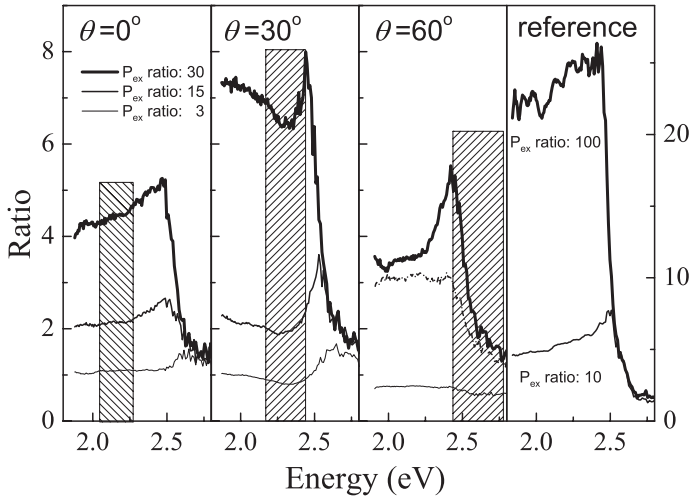

Figure 15. Enhancement of the spontaneous emission of a Perylen dye at the edges of the stop-band in Perylen doped SnS_2 inverted opal for power increments of 3, 15 and 30 (P_{ex} ratio) Shadowed regions shows the position of the stop-band at the different angles of observation. The ratio spectra for an unstructured reference film (power ratio 10 and 100) is shown in the rightmost panel.

The RI contrast can become extremely large for frequencies around the plasma frequency. Silver is the first metal to come to mind for energies in the region of 2.4–4.0 eV, having the zero crossing of the real part of the RI around 3.78 eV.

Fig. 16 shows reflectance measurements for a SiO_2 bulk opal undertaken prior and after infilling with silver. A clear blueshift of the reflectance peak can be seen. This is attributed to a decease of the effective refractive index of the whole structure due to the silver infilling. The magnitude of the shift of 0.21 eV corresponds to a decrease of the RI inside of the voids from 1 (air) to 0.70 due to the silver-infill. The fraction of the voids that has been occupied by silver and whether the metal forms a cermet or a network topology has not yet been confirmed. However, the topology of metal component is an important issue since the PBG of a MD PhC of cermet topology resembles that of a DD PhCs. Similar transmission spectra of opals infilled with a small amount of Ag nanoparticles exhibit a blueshift and a widening of the stop-band have been observed by Zhou et al. [47].

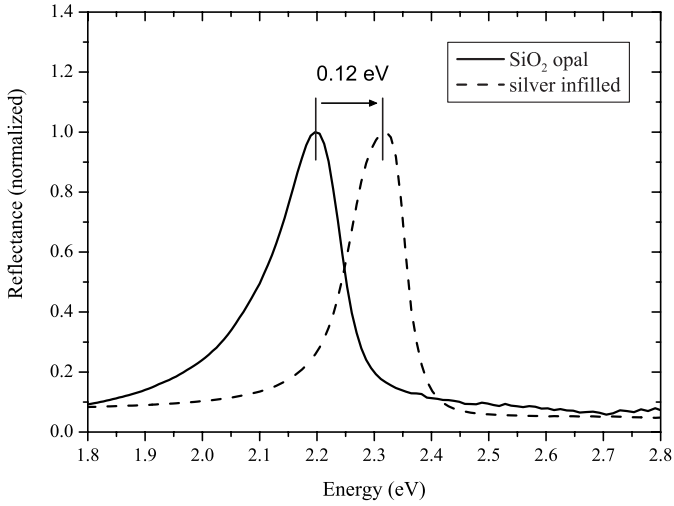

Figure 16. Reflectance spectra of SiO_2 bulk-opal prior (solid line) and after (dashed line) infilling with silver. The spectra were taken at near-normal incidence ($\theta = 6°$).The blue-shift is attributed to the reduction of the effective RI induced by the silver.

14. SUMMARY

Materials science using opals as 3D photonic crystals is still in its infancy. Structures have been prepared from materials with different RIs and filling factors, including some additional features like emitting species (dyes, rare earth ions, etc.) or special coatings to study the changes in PBG and PBG-related properties of the material.

Disorder is one of the most severe problems to be overcome in self-assembled systems, which is partly solved by application of thin film opals. Modifications of opaline photonic crystals, as polymer-based self-assembled opaline systems offer some flexibility, e.g., in choosing suitable dyes as dopants and to match the emission properties of embedded dyes with the PBG. On the other hand, the relatively low RIC of these structures limits their use to applications, where a partial PBG is sufficient.

To reach a full PBG it is necessary to go for inverted structures of high RI semiconductors or dielectrics. Different photonic crystals offer specific advantages and disadvantages:

1. Inverted opals. So far those routinely produced are TiO_2 and SnS_2 opaline structures. They offer high refractive index contrast combined with the possibility to obtain the optimal filling fraction,

thus reaching closely a complete photonic bandgap in the visible. Unfortunately, the crystalline quality of these replicas is in general lower compared to the opal templates. Additionally the operating range of all-dielectric photonic crystals is restricted by the absorption edge of the material — either to NIR for Si and Ge inverted opals or to the red part of the visible spectrum (SnS_2).

2. Metallodielectric photonic crystals. This is an interesting alternative to approach a complete PBG material as compared with DD PhCs. Almost no experiments have been undertaken with MD photonic crystals in the visible regime so far. But they might have a bright future, since they presumably offer a way to reach a robust and omnidirectional photonic bandgap.
3. Opal based light sources. Although they do not offer a full photonic bandgap yet, strong changes of the directionality of the emission have been observed compared with the pure dye-polymer films in accord with the anisotropy of the stop-band.

Thin film opals at present still not reached the state of device applications but they offer a benchmark to test novel concepts for future optoelectronics.

ACKNOWLEDGMENT

Part of this work has been supported by the EU IST Project PHOBOS, Grant No. 19009.

REFERENCES

1. Bykov, V. P., "Spontaneous emission in a periodic structure," *Sov. Phys. JETP*, Vol. 35, 269, 1972.
2. Yablonovich, E., "Inhibited spontaneous emission in solid-state physics and electronics," *Phys. Rev. Lett.*, Vol. 58, 2059, 1987. John, S., "Strong localization of photons in certain disordered dielectric superlattices," *Phys. Rev. Lett.*, Vol. 58, 2486, 1987.
3. Noda, S., N. Yamamoto, M. Imrada, H. Kobayashi, and M. Okato, "Alignment and stacking of semiconductor photonic bandgaps by wafer-fusion," *J. Lightwave Technol.*, Vol. 17, 1948, 1999.
4. Cuisin, C., A. Chelnokov, J. M. Lourtioz, D. Decanini, and Y. Chen, "Fabrication of three-dimensional photonic structures with submicrometer resolution by x-ray lithography," *J. Vac. Sci. Technol. B*, Vol. 18, 3535, 2000.

5. Wang, K., A. Chelnokov, S. Rowson, P. Garoche, and J. M. Lourtioz, "Focused-ion-beam etching in macroporous silicon to realize three-dimensional photonic crystals," *J. Phys. D: Appl. Phys.*, Vol. 33, L119, 2000.
6. Lin, S. Y. and J. G. Fleming, "A three dimensional optical photonic crystal," *J. Lightwave Technol.*, Vol. 17, 1944, 2000.
7. Champbell, M., D. N. Sharp, M. T. Harrison, R. G. Denning, and A. J. Turberfield, "Fabrication of photonic crystals for the visible spectrum by holographic lithography," *Nature*, Vol. 404, 53, 2000.
8. Kuramochi, E., M. Notomi, T. Tamamura, T. Kawashima, S. Kawakami, J. Takahashi, and C. Takahashi, "Drilled alternating-layer structure for three-dimensional photonic crystals with a full band gap," *J. Vac. Sci. Technol. B*, Vol. 18, 3510, 2000.
9. Stöber, W., A. Fink, and E. Bohn, "Controlled growth of monodisperse silica spheres in the micron size range," *J. Colloid. Interface Sci.*, Vol. 26, 62, 1968.
10. Míguez, H., F. Meseguer, C. López, A. Mifsud, J. S. Moya, and L. Váazquez, "Evidence of fcc crystallization of SiO_2 nanospheres," *Langmuir*, Vol. 13, 6009, 1997.
11. Holgado, M., F. García-Santamaría, A. Blanco, M. Ibisate, A. Cintas, H. Míguez, C. J. Serna, C. Molpeceres, J. Requena, A. Mifsud, F. Meseguer, and C. López, "Electrophoretic deposition to control artificial opal growth," *Langmuir*, Vol. 15, 4701, 1999.
12. Vlasov, Yu. A., V. N. Astratov, A. V. Baryshev, A. A. Kaplyanskii, O. Z. Karimov, and M. F. Limonov, "Manifestation of intrinsic defects in optical properties of self-organized opal photonic crystals," *Phys. Rev. E*, Vol. 61, 5784, 2000.
13. Xia, Y., B. Gates, Y. Yin, and Y. Lu, "Monodispersed colloidal spheres: old Materials with new applications," *Adv. Mat.*, Vol. 12, 693, 2000.
14. Rogach, A., A. Susha, F. Caruso, G. Sukhorukov, A. Kornowski, S. Kershaw, H. Möhwald, A. Eychmüller, and H. Weller, "Nano- and microengineering: 3-D colloidal photonic crystals prepared from sub-μm-sized polystyrene latex spheres pre-coated with luminescent polyelectrolyte/nanocrystal shells," *Adv. Mat.*, Vol. 12, 333, 2000.
15. Astratov, V. N., V. N. Bogomolov, A. A. Kaplyanskii, A. V. Prokofiev, L. A. Samoilovich, S. M. Samoilovich, and Yu. A. Vlasov, "Optical spectroscopy of opal matrices with CdS embedded in its pores: Quantum confinement and photonic bandgap effects," *Il Nuovo Cimento*, Vol. 17D, 1349, 1995.

16. Romanov, S. G., A. V. Fokin, V. V. Tredijakov, V. Y. Butko, V. I. Alperovich, N. P. Johnson, and C. M. Sotomayor Torres, "Optical properties of ordered three-dimensional arrays of structurally confined semiconductors," *J. Crystal Growth*, Vol. 159, 857, 1996.
17. Vlasov, Yu. A., M. Deutsch, and D. J. Norris, "Single-domain spectroscopy of self-assembled photonic crystals," *Appl. Phys. Lett.*, Vol. 76, 1627, 2000.
18. Van Blaaderen, A., R. Ruel, and P. Wiltzius, "Template-directed colloidal crystallization," *Nature*, Vol. 385, 321, 1997.
19. Goodwin, J. W., J. Hearn, C. C. Ho, and R. H. Ottewill, "Studies on the preparation and characterisation of monodisperse polystyrene latices," *Colloid Polym. Sci.*, Vol. 252, 464, 1974.
20. Gates, B., D. Qin, and Y. Xia, "Assembly of nanoparticles into opaline structures over large areas," *Adv. Mat.*, Vol. 11, 466, 1999.
21. Kralchevsky, P. A., N. D. Denkov., V. N. Paunov, O. D. Velev, I. B. Ivanov, H. Yoshimura, and K. Nagayama, "Formation of two-dimensional colloid crystals in liquid films under the action of capillary forces," *J. Phys.: Condens. Matter*, Vol. 6, A395, 1994.
22. Amos, R., J. G. Rarity, P. R. Tapster, and T. J. Shepherd, "Fabrication of large-area face-centered-cubic hard-sphere colloidal crystals by shear alignment," *Phys. Rev. E*, Vol. 61, 2929, 2000.
23. Vos, W. L. and H. M. van Driel, "Higher order Bragg diffraction by strongly photonic *fcc* crystals: onset of a photonic bandgap," *Physics Letters A*, Vol. 272, 101, 2000.
24. Bertone, J. F., P. Jiang, K. S. Hwang, D. M. Mittleman, and V. L. Colvin, "Thickness dependence of the optical properties of ordered silica-air and air-polymer photonic crystals," *Phys. Rev. Lett.*, Vol. 83, 300, 1999. Romanov, S. G., T. Maka, C. M. Sotomayor Torres, M. Müller, and R. Zentel, "Thin film photonic crystals," *Synthetic Metals*, Vol. 116, 475, 2001.
25. Reynolds, A., F. López-Tejeira, D. Cassagne, F. J. García-Vidal, C. Jouanin, and J. Sánchez-Dehesa, "Spectral properties of opal-based photonic crystals having a SiO_2 matrix," *Phys. Rev. B.*, Vol. 60, 11422, 1999.
26. Pendry, J. B. and A. MacKinnon, "Calculation of photon dispersion relations," *Phys. Rev. Lett.*, Vol. 69, 2772, 1992. Bell, P. M., J. B. Pendry, L. M. Moreno, and A. J. Ward, "A program for calculating photonic band structures and transmission coefficients of complex structures," *Comp. Phys. Comm.*, Vol. 85, 36, 1995.

27. Van Driel, H. M. and W. L. Vos, "Multiple Bragg wave coupling in photonic band-gap crystals," *Phys. Rev. B*, Vol. 62, 9872, 2000.
28. Romanov, S. G., T. Maka, C. M. Sotomayor Torres, M. Müller, R. Zentel, D. Cassagne, J. Manzanares-Martinez, and C. Jouanin, "Diffraction of light from thin-film polymethylmethacrylate opaline photonic crystals," *Phys. Rev. E*, Vol. 63, 056603, 2001.
29. Sözüer, H. S., J. W. Haus, and R. Inguva, "Photonic bands: Convergence problems with the plane-wave method," *Phys. Rev. B*, Vol. 45, 13962, 1992.
30. Busch, K. and S. John, "Photonic band gap formation in certain self-organizing systems," *Phys. Rev. E*, Vol. 58, 3896, 1998.
31. Wijnhoven, JEGJ and W. L. Vos, "Preparation of photonic crystals made of air spheres in titania," *Science*, Vol. 281, 802, 1998.
32. Blanco, A., E. Chomski, S. Grabtchak, M. Ibisate, S. John, S. W. Leonard, C. Lopez, F. Meseguer, H. Míguez, J. P. Mondia, G. A. Ozin, O. Toader, and H. M. van Driel, "Large-scale synthesis of a silicon photonic crystal with a complete three-dimensional bandgap near 1.5 micrometres," *Nature*, Vol. 405, 437, 2000.
33. Doosje, M., B. J. Hoerders, and J. Knoester, "Photonic bandgap optimization in inverted fcc photonic crystals," *J. Opt. Soc. Am. B*, Vol. 17, 600, 2000.
34. Romanov, S. G., H. M. Yates, M. E. Pemble, and R. M. de la Rue, "Impact of GaP layer deposition upon photonic bandgap behaviour of opal," *J. Phys.: Cond. Matter*, Vol. 12, 339, 2000.
35. Müller, M., R. Zentel, T. Maka, S. G. Romanov, and C. M. Sotomayor Torres, "Photonic crystal films with high refractive index contrast," *Adv. Mat.*, Vol. 12, 1499, 2000.
36. Vlasov, Yu. A., N. Yao, and D. J. Norris, "Synthesis of photonic crystals for optical wavelengths from semiconductor quantum dots," *Adv. Mat.*, Vol. 11, 165, 1999.
37. Megens, M., JEGJ Wijnhoven, A. Lagendijk, and W. L. Vos, "Light sources inside photonic crystals," *J. Opt. Soc. Am. B*, Vol. 16, 1403, 1999.
38. Romanov, S. G., A. V. Fokin, and R. M. de la Rue, "Eu^{3+} emission in an anisotropic photonic bandgap environment," *Appl. Phys. Lett.*, Vol. 76, 1656, 2000.
39. Bogomolov, V. N., S. V. Gaponenko, I. N. Germanenko, A. M. Kapitonov, E. P. Petrov, N. V. Gaponenko, A. V. Prokofiev, A. N. Ponyavina, N. I. Silvanovich, and S. M. Samoilovich, "Photonic band gap phenomenon and optical properties of

artificial opals," *Phys. Rev. E*, Vol. 55, 7619, 1997.

40. John, S., "Localization of light — theory of photonic band gap materials," *Photonic Band Gap Materials*, C. M. Soukoulis (ed.), 563–665, Kluwer Academic Publishers, Dordrecht, 1995.
41. Yamasaki, T. and T. Tsutsui, "Spontaneous emission from fluorescent molecules embedded in photonic crystals consisting of polystyrene microspheres," *Appl. Phys. Lett.*, Vol. 72, 1957, 1998.
42. Romanov, S. G., T. Maka, C. M. Sotomayor Torres, M. Müller, and R. Zentel, "Emission properties of dye-polymer-opal photnoic crystals," *J. Lightwave Technol.*, Vol. 17, 2121, 1999.
43. Suzuki, T. and P. K. L. Yu, "Emission power of an electric dipole in the photonic band structure of the fcc lattice," *J. Opt. Soc. Am. B*, Vol. 12, 570, 1995.
44. Kosaka, H., T. Kawashima, A. Tomita, M. Notomi, T. Tamamura, T. Sato, and S. Kawakami, "Superprism phenomena in photonic crystals," *Phys. Rev. B*, Vol. 58, R10096, 1998.
45. Purcell, E. M., "Spontaneous emission probabilities at radio frequencies," *Phys. Rev.*, Vol. 69, 681, 1946.
46. Moroz, A., "Three-dimensional complete photonic-band-gap structures in the visible," *Phys. Rev. Lett.*, Vol. 83, 5274, 1999.
47. Zhou, J., Y. Zhou, S. L. Ng, H. X. Zhang, W. X. Que, Y. L. Lam, Y. C. Chan, and C. H. Kam, "Three-dimensional photonic band gap structure of a polymer-metal composite," *Appl. Phys. Lett.*, Vol. 76, 3337, 2000.
48. Johnson, S. G. and J. D. Joannopoulos, "Block-iterative frequency-domain methods for Maxwell's equations in a planewave basis," *Optics Express*, Vol. 8, 173, 2001.